Evaluation of intermolecular interactions of hydrogels : Experimental study and constitutive modeling

Makoto Uchida[1*], Tamon Ichikawa[1], Hiroto Sato[1], Yoshihisa Kaneko[1],
Dai Okumura[2], Mokarram Hossain[3]

[1]Osaka Metropolitan University, [2]Nagoya University, [3]Swansea University, *Email: m_uchida@omu.ac.jp

Abstract

The mechanical properties of hydrogels are significantly influenced by the solvent content. In particular, inelastic deformation occurs in dried hydrogels. In this study, we quantitatively evaluated the inelastic deformation of a hydrogel introduced by intermolecular interactions under uniaxial tensile loading-unloading tests and established a visco-hyperelastic model describing the experimentally observed inelastic behavior based on the transient network theory. The development of the strain field during the test was measured using digital image correlation (DIC) method, and the relationship between the true stress and the true strain was evaluated using the obtained strain field. A significant difference between the loading and the unloading responses was observed for the dried hydrogel specimens. This result indicates that intermolecular interactions induce irreversible deformation when the intermolecular chain distance is smaller. A non-dimensional parameter corresponding to the intermolecular chain distance was introduced to describe the irreversible response of the hydrogel observed in the experimental study. This parameter is a function of the densities of molecular chains, number of segments per chain, and stretching accompanied by swelling and drying. A visco-hyperelastic model was established by introducing the proposed parameter into the transient network theory. The proposed model qualitatively and quantitatively reproduced the experimentally observed features of the mechanical response of the hydrogel.

Keywords: hydrogel, swelling, drying, inelastic, visco-hyperelastic, transient network, intermolecular interaction

1 Introduction

Hydrogels are widely used in biomedical materials [Li et al., 2023; Ajam et al., 2024; Cai et al., 2024] and soft actuators [Apsite et al., 2022; Chen et al, 2023; Khalid et al., 2024] because of their excellent properties, such as top-level softness akin to most biological tissues, biocompatibility. Another essential property is that hydrogels can contain a specific amount of solvent in their molecular chain networks depending on the densities of the molecular chains and crosslinks, chemical compatibility, and external stress state. The volume fraction of the solvent significantly influences the mechanical properties of a hydrogel. Hence, an accurate prediction of the variations in mechanical performance with the solvent content is required to effectively utilize these unique behaviors in their applications.

Swelling in the elastomer can be described using the classical Flory-Rehner model, which estimates the balance of the free-energy function consisting of the mechanical stretching and mixing of the polymer and solvent [Flory and Rehner, 1943; Boyce and Arruda, 2001; Chester and Annand, 2010]. To accurately describe the variation in stiffness due to swelling, Okumura et al. introduced scaling parameters to estimate the strain energy functions [Okumura et al., 2016, 2018]. This model was applied to evaluate the swelling limit [Okumura and Chester, 2018], irregular elasticity of high- and low-molecular-weight swollen gels [Kawai et al., 2021], In addition, the swelling of the gel affects not only its mechanical properties, but also its unique characteristics, such as multiaxial behaviors [Khiêm et al., 2019; Xiao et al., 2021; Esmaeili et al., 2023], wrinkling and patterning of bilayer gels [Kikuchi et al., 2022; Nagashima et al., 2023], and anisotropic electromechanical responses [Hatami-Marbini and Mehr, 2022].

In addition to the above studies, the authors investigated the effect of swelling on the mechanical response, and a constitutive model was established based on the molecular chain network theory [Uchida et al., 2019a]. In the proposed model, the density and pre-stretching of the molecular chain were described as a function of the swelling amount. Although the proposed model could represent the decreases in initial stiffness and critical stretch with increasing solvent content observed in the experimental study, it underestimated the degree of stress change accompanied by the swelling. This result indicates that the mechanical properties of hydrogels cannot be explained only by the density and pre-stretching of the molecular chain owing to the penetration of the solvent.

In the above works, the mechanical behavior of hydrogel was assumed as a time-independent hyperelastic material. In the hydrogels containing sufficient solvent in the molecular chain network, the distance between molecular chains is expanded by the solvent, which results in weaker intermolecular chain interaction. Therefore, the viscous feature owing to the intermolecular chain interaction is not observed. In contrast, apparent time-dependent behaviors are observed in double-network (DN) hydrogels, which have a secondary-bonded network maintained by ion bonds added to the covalently bonded major network [Javadi et al., 2020; Lei et al., 2020; Jin et al., 2022; Eshaghi and Weiss, 2022; Cai et al., 2024]. This time-dependent mechanical behavior is induced by inelastic dissipation during the irreversible deformation of the secondary-bonded network. Based on this mechanism, the viscoelastic constitutive equations for DN hydrogels were proposed [Mao et al., 2017; Zhu and Zhang, 2020; Javadi et al; 2020; Zhan et al., 2024]. In these models, the inelastic behaviors of DN hydrogels were described by using the free energy, including energy dissipation owing to the change in the secondary-bonded network.

Even in the single-network (SN) hydrogels, the viscoelastic property was observed in the dried or deswollen hydrogels [Lei et al., 2019; Bosnjak et al., 2019; Matsubara et al., 2024; Lin et al., 2024]. In contrast to the DN hydrogel, an energy dispassion related to the secondary-bonded network is not included in the SN hydrogel. Nevertheless, the irreversible responses were observed in the SN hydrogels with lower solvent contents. Bosnjak et al. [2019] represented the inelastic behaviors of virgin and swollen polymeric gels by a viscoelastic model with parameters separately calibrated for every gel with different solvent contents. Lin et al. [2024] introduced a power-law relationship between solvent contents and initial modulus to predict the inelastic behaviors of hydrogels with different solvent contents. These phenomenological models could represent the irreversible responses of single-network hydrogels during the loading-unloading cycle. The inelastic deformation of SN hydrogel was interpreted by the intermolecular-chain interaction. Lei et al. [2019, 2021] represented the nonlinear stress-strain response of SN hydrogels by the intermolecular-chain friction. In this model, the increase in the viscoelasticity with decreasing solvent contents was explained by insufficient lubrication between polymer chains for the thinner solvent layer. Liu et al. (2025) proposed a visco-hyperelastic model characterized by the intermolecular-chain slippage with three-dimensional chain conformation to predict the effect of the strain rate on the irreversible loading-unloading response

of SN hydrogel. Although the effect of the solvent contents on the irreversible deformation was not discussed in these studies, the interpretation of the deformation mechanism based on the molecular chain kinetics helps in understanding the inelastic deformation of hydrogels.

The important point in the inelastic deformation of hydrogel is that the magnitude of the viscosity of the material is characterized by solvent contents. This is due to the decrease in the intermolecular distance with decreasing solvent contents during drying and deswelling, which increases the intermolecular interactions. The time-dependent mechanical behaviors such as creep and stress relaxation are critical characteristics of the polymeric materials. Quantitative measurement of the viscosity in the material related to its microscopic characteristics, such as densities of molecular chain and crosslink, may improve the understanding and prediction of the time-dependent mechanical behaviors of the polymeric materials.

The time-dependence in the mechanical behaviors of the polymeric materials above and below the glass transition temperature, T_g, are different. Above T_g, which corresponds to the rubbery state, the polymer macrostructure is assumed to exhibit affine deformation with the molecular chain network. The entropic elasticity model is typically employed to describe the hyperelastic behavior of rubbery materials [Kuhn and Grün, 1942; Ogden, 1972; Arruda and Boyce, 1993]. The time dependence of mechanical behavior is a critical issue for rubbery materials, and many models were developed to represent its viscoelastic (VE) behavior. [Fazekas and Goda, 2021; Tayeb et al., 2022; Anssari-Benam and Hossain, 2023; Alkhoury et al., 2024]. To explain the VE behavior of rubber related to the intermolecular chain interaction, the transient-network (TN) theory was proposed [Tanaka and Edward, 1992; Vernerey et al., 2017; Sridhar and Vernerey, 2020]. In the TN theory, the inelastic response of rubber was represented by the development of the transient network, which is constructed by the weaker intermolecular connection.

In contrast, viscoelastic-viscoplastic (VE-VP) deformation occurs below T_g because the interaction between the molecular chains constrains the rotation of the segments in the chain. Several pioneering nonlinear models, such as the Eyring flow and rubbery elasticity coupling model [Haward and Tackray, 1968], double-kink model [Argon, 1973], and true strain-softening model [Boyce et al., 1988], have been proposed to describe the inelastic deformation of glassy polymer, and related studies are still ongoing [Lan et al., 2022, 2024; Alves et al., 2023; Anssari-Benam

2024a, 2024b]. Uchida et al. developed the VE-VP TN theory to reproduce the time- and temperature-dependent behaviors of glassy and semi-crystalline polymers [Uchida et al., 2019b, 2022, 2024; Yoshida et al., 2022]. In this model, the molecular chain network is decomposed into a crosslinked fixed network and a transient network with weaker bonds, and the density of the weaker bonds continuously changes with the temperature, external stress, and flow of the polymer. As mentioned, the TN theory, which relates time-dependent behavior and intermolecular chain interaction, successfully reproduced the time-dependent behaviors in the rubber, glassy polymer, and semi-crystalline polymer. Although the degrees differ, the time-dependent behaviors of polymers above and below T_g are induced by common mechanisms based on intermolecular interactions.

Because viscoelastic responses in the dried and deswollen hydrogels were also driven by the intermolecular chain interaction, the TN theory is expected to explain the time-dependent behavior of the hydrogel. Here, the magnitude of the viscosity of hydrogel can be changed by composition and solvent contents. In this study, we attempt to introduce the quantity characterized by the molecular chain network based on the experimental study and to describe the inelastic deformation of hydrogel using the introduced quantity with TN theory. This may provide important information for understanding the rate-sensitivity of the polymers and accurate prediction of time-dependent performance such as creep and relaxation. As-prepared, swollen, and dried hydrogel specimens were prepared with different hydrogel compositions to vary the intermolecular distances. To evaluate the effect of the microscopic characteristics of hydrogen on the inelastic deformation of the hydrogel, we perform uniaxial tensile loading-unloading tests of hydrogel specimens with different intermolecular distances. The loading and unloading responses were similar when the molecular chains deformed affinely, independent of the surrounding chains in the swollen hydrogel. In contrast, differences in the response may occur with decreasing the intermolecular chain distances in the dried hydrogels and/or those with a higher monomer density. By evaluating the irreversibility of the loading and unloading responses, an intermolecular chain distance parameter was introduced to characterize the inelastic deformation behavior of the hydrogel. Finally, we establish a visco-hyperelastic model describing the experimentally observed inelastic behavior based on the TN theory.

In Section 2, the experimental method and results of the uniaxial tensile loading-unloading test are explained,

and the irreversibility of the mechanical behaviors of the hydrogels is demonstrated. In Section 3, the intermolecular chain distance parameter characterizing the inelastic behavior of the hydrogel is introduced. Through comparisons between the experimental and simulation results, the inelastic deformation mechanisms of the hydrogels related to the intermolecular interactions are discussed. Finally, a visco-hyperelastic constitutive model for hydrogel for a wider range of solvent contents from dried to swollen states is proposed using the introduced intermolecular chain distance parameter.

2 Experiment

2.1 Experimental method

The polyacrylamide hydrogel used in this study was composed of acrylamide (AAm) and N,N'-methylenebisacrylamide (BIS). After dissolving the AAm and BIS, which are a monomer and a cross-linker, respectively, in water, polymerization was performed using ammonium persulfate (APS) and tetramethylethylenediamine (TMEDA) as the initiator and accelerator, respectively. Samples with different Aam and BIS contents were prepared to evaluate the effect of the molecular chain and crosslink densities on the mechanical behavior of the hydrogel. The obtained specimens are referred to as PAG $C_x - C_y$, where C_x and C_y are the weight ratios (wt%) of AAm and BIS, respectively, with respect to the total weight of the hydrogel. The compositions of the hydrogels prepared in this study are listed in Table 1.

Table 1 Compositions and swelling ratios of hydrogel used in this study

	AAm [g]	BIS [mg]	APS [mg]	TMEDA [mL]	H_2O [mL]	V_{SW}/V_0
PAG $20-0.01$	2.4	1.2	17.1	0.0449	9.53	5.29
PAG $20-0.05$	2.4	6.0	17.1	0.0449	9.53	3.52
PAG $20-0.1$	2.4	12.0	17.1	0.0449	9.53	2.44
PAG $30-0.01$	3.6	1.2	17.1	0.0449	8.33	6.14
PAG $30-0.05$	3.6	6.0	17.1	0.0449	8.33	3.29
PAG $30-0.1$	3.6	12.0	17.1	0.0449	8.33	3.14

Specimens with dimensions of 30 mm (length)× 10 mm (width)× 1 mm (thickness) were formed using silicone molds. As-prepared (AP), fully swollen (SW), and dried specimens were prepared for all hydrogel compositions to obtain the hydrogel specimens with different intermolecular distances. The weight increase ratios of the swollen specimens for all hydrogel compositions are listed in Table 1. Dried specimens were obtained by drying the AP specimens in atmosphere until their weight decreased to 80 % and 60 % of the initial weight. $\_AP$, $\_SW$, _0.8, and _0.6 were added for AP, SW, and dried until 80 wt% and 60 wt% specimens, respectively, to perform the post-treatment of the specimen.

Uniaxial tensile loading and unloading tests were performed using an automatic vertical-type servo tensile testing machine (JSV-H I000, Japan Instrumentation System Co., Ltd.). Tensile forces were measured using a digital force gauge with a resolution of 0.001 N (HF-1, Japan Instrumentation System Co., Ltd.), which was attached to the testing machine. Water in the hydrogel specimen gradually decreases during the atmosphere exposure by evaporation. The decrease rate in the weight ratio of the specimens employed in this study were ranged approximately 0.001 to 0.002 wt%/min, depending on the specimen configuration. The solvent in the polymer network in the hydrogel evaporates during air exposure. Approximately 0.175 [wt%/min] and 0.273 [wt%/min] weight decreases were observed for PAG $20-0.01$_AP and PAG $30-0.1$_AP, respectively. If the total time for the loading-unloading process is long, the change in the response owing to the weight decrease during the test may be included in the result. Therefore, we performed the loading-unloading test with a relatively faster stroke speed of $\dot{U} = 20$ mm/min. In the previous study, hydrogel specimens with various compositions and solvent contents showed approximately 1.8 to 7.5 of maximum stretch (approximately 0.6 to 2.0 of true strain). In this study, an initial holding distance and a maximum tensile displacement of 15 mm and 20 mm, respectively, which corresponds to the maximum stretch of 1.75, was employed to compare the loading-unloading process of hydrogel specimens with different solvent contents and compositions in the unified deformation range.

Because of the relative slip between the interface of the hydrogel and holding tool during the loading-unloading tensile tests, a fictional irreversible strain occurred when crosshead displacement was employed to evaluate the strain. Therefore, the strain in the hydrogel specimens was measured using a DIC. netDIC method [Uchida and Tada, 2011] was employed to accurately measure an extremely large strain in the hydrogel during the tensile tests. In the netDIC, the deformation of the subset referencing the brightness distribution around the point of interest is approximated using displacements of the surrounding measurement points. It enables stable and accurate displacement measurements even under large deformations and high-strain gradient conditions. For the DIC measurements, a dot-array pattern was employed for the brightness distribution, which was applied to the surface of the hydrogel specimen using a watercolor ink pen, as shown in Fig. 1. Digital images of the specimen surfaces were captured using a digital single-lens reflex camera (Body: K20, Pentax Co. Ltd., Lens: DFA Macro SO mm F2.8, Pentax Co. Ltd.) in intervals of 15 s. The spatial resolution of the digital image was approximately 15 μm/pixel. In the displacement measurement, we employed 40×40 pixels for the subset size, and the deformation of the subset was approximated by the linear function of the coordinate using ten surrounding measurement points. The repetitive calculation was performed until the change in the displacement became smaller than 1×10^{-5} pixel. The

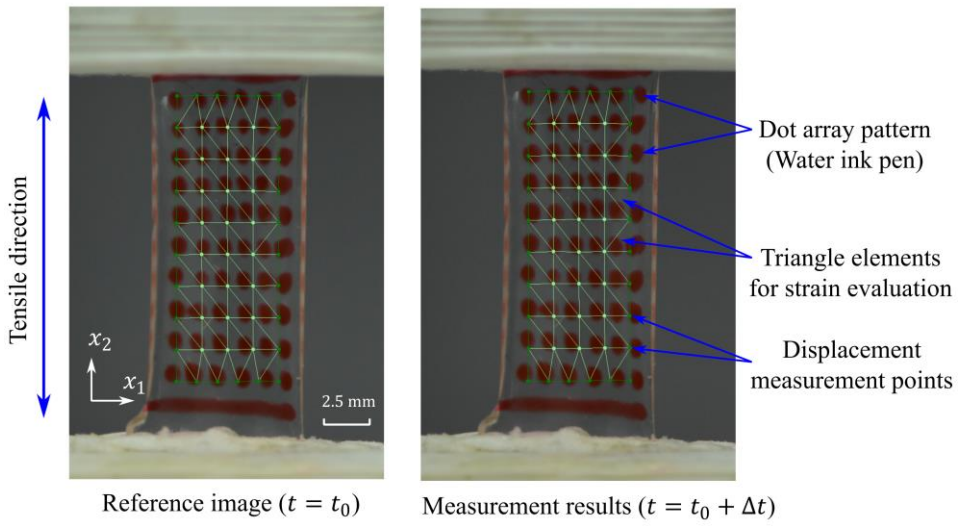

Fig. 1 Sequential digital images of a hydrogel specimen during the test. A dot-array pattern was provided on the surface of the hydrogel specimen using a watercolor ink pen. Displacement measurement points were generated around the dots, and the triangular element mesh was created using the displacement measurement points to evaluate the development of the strain field.

error in the displacement detection for netDIC is smaller than 0.01 pixel [Uchida and Tada, 2011] (0.15 μm in the digital image), which is sufficiently smaller than the displacement of the hydrogel.

The strain field was evaluated after determining the displacements of the measurement points. First, a triangular element mesh was generated using the displacement measurement point. Subsequently, the two-dimensional components of the deformation gradient tensor were calculated for the triangular elements using the displacements vectors on the nodal points, similar to the conventional finite element method (FEM) scheme. The deformation gradient, $\boldsymbol{F}$, is expressed as follows:

$$\boldsymbol{F} = \frac{\partial \boldsymbol{x}}{\partial \boldsymbol{X}} = \boldsymbol{I} + \frac{\partial \boldsymbol{u}}{\partial \boldsymbol{X}} \tag{1}$$

The left Cauchy -Green stretch tensor, $\boldsymbol{V}$, is then expressed as follows:

$$\boldsymbol{V}^2 = \boldsymbol{F} \cdot \boldsymbol{F}^T \tag{2}$$

The local true strain tensor was calculated using Eq. (3)

$$\boldsymbol{\varepsilon} = \ln \boldsymbol{V} \tag{3}$$

During the tensile tests, uniaxial tension was applied to the hydrogel specimen in x_2 direction. The global tensile stretch $\bar{\lambda}$ and global true stress $\bar{\sigma}_{22}$ in the tensile direction were then calculated as follows:

$$\bar{\lambda} = \exp\left(\frac{1}{V}\int_V \varepsilon_{22} dV\right) \tag{4}$$

$$\bar{\sigma}_{22} = \frac{F}{A_0}\bar{\lambda} \tag{5}$$

where V is the volume of the displacement evaluation region, F is the tensile load, and A_0 is the initial cross-section of the hydrogel specimen. The initial cross-sections of the swollen and dried hydrogel specimens were estimated using the weight change equation as follows:

$$A_0 = A_0^{AP}\left(\frac{W}{W_0}\right)^{\frac{2}{3}} \tag{6}$$

where A_0^{AP} is the initial cross-section of the AP specimen, and W_0 and W are the weights of the specimen before and after swelling or drying, respectively.

2.2 Experimental results

Experimental results of the uniaxial tensile loading-unloading tests of the hydrogel are presented and discussed in this section. Fig. 2 shows the development of the strain field measured using DIC during the tests for (a) PAG $20-0.01\_AP$, (b) SW, (c) 0.8, and (d) 0.6. The values in Fig. 2 are the applied stresses, loading (L) and unloading (UL), respectively. Although a slight strain distribution was observed, the strain in the DIC measurement area, which was apart from the holding area, was almost uniform. The strain field after unloading until the zero-stress state differed from that prior to the loading. In particular, a significant residual strain was observed in dried hydrogels PAG 20 -0.01_0.8 and 0.6. In contrast, the residual strain in the swollen hydrogel was relatively small. This result indicated that an irreversible deformation was introduced owing to the intermolecular interactions during the loading-unloading cycle in the dried hydrogels.

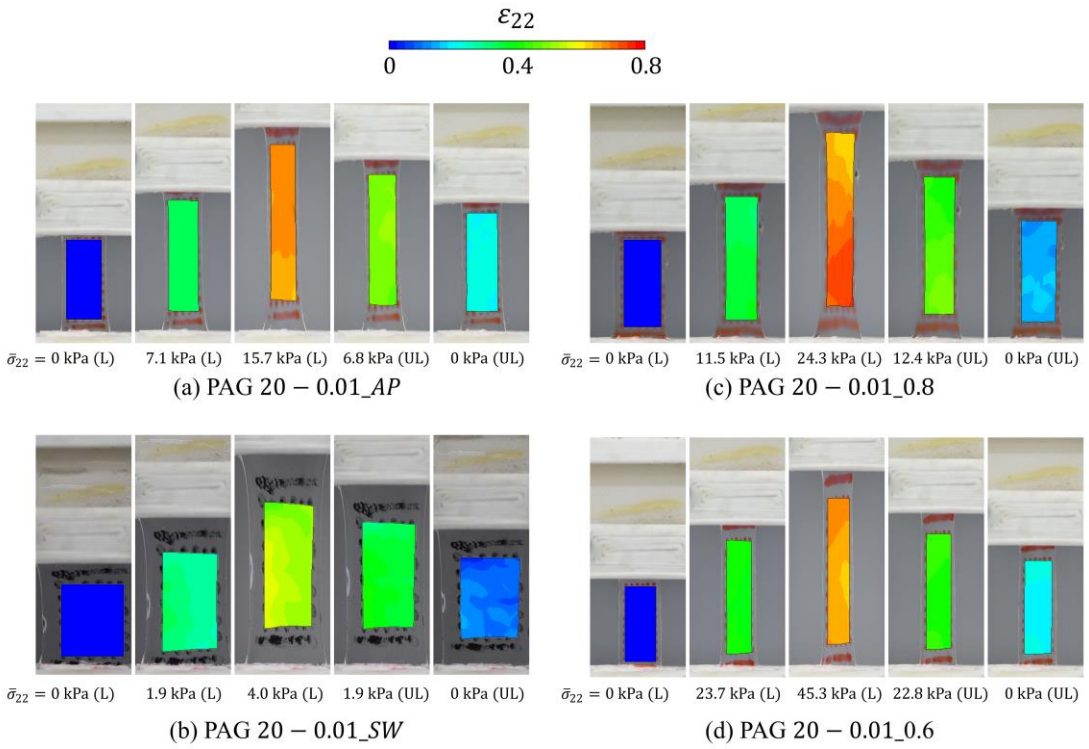

Fig. 2 Development of strains during the uniaxial tensile loading-unloading tests on (a) PAG $20-0.01\_AP$, (b) SW, (c) 0.8, and (d) 0.6. The values in the graphs represent applied stresses, and (L) and (UL) indicate "loading" and "unloading", respectively.

Using the strain measured using DIC and the tensile load, the relationships between the true strain and stretch were evaluated using Eqs. (4) and (5), respectively. The results obtained for all hydrogel conditions are presented in Fig. 3. Fig. 3 (a)-(f) presents the results for PAG $20-0.01$, $20-0.05$, $20-0.05$, $30-0.01$, $30-0.05$, and $30-0.1$, respectively. The black, red, blue, and orange lines represent PAG C^x-C^y_0.6, 0.8, AP, and SW, respectively. It should be noted that the scales of the vertical axes of (a)-(c) and (d)-(f) are different. The results of the loading-unloading test on PAG $30-0.1\_SW$ could not be obtained because the specimen fractured in the earlier strain range. With decreasing solvent content, the stress increased for all hydrogels. Furthermore, with an increase in the initial densities of the monomer and cross-linker, the slope of the curve and the maximum stress increased. In addition, the dried hydrogel exhibited a pronounced irreversible response during the loading-unloading cycle. The difference between the loading and unloading curves increased with decreasing the solvent content. In contrast, the swollen hydrogels exhibited almost the same curves during the loading and unloading processes. Although the increase in the stiffness of hydrogels with decreasing solvent content can be explained by the increasing density, the degree of the stress difference between AP and SW hydrogels was underestimated in the previous study [Uchida et al., 2019a]. Meanwhile, Brighenti et al. [2024] suggested that the intermolecular hydrogen bonds influenced the stiffness of the hydrogel. In addition, a pronounced irreversible deformation was observed during the loading-unloading cycle in the dried hydrogels. These indicate that intermolecular interactions such as the hydrogen bonds and van der Waals interaction are introduced in the hydrogels with a shorter intermolecular chain distance.

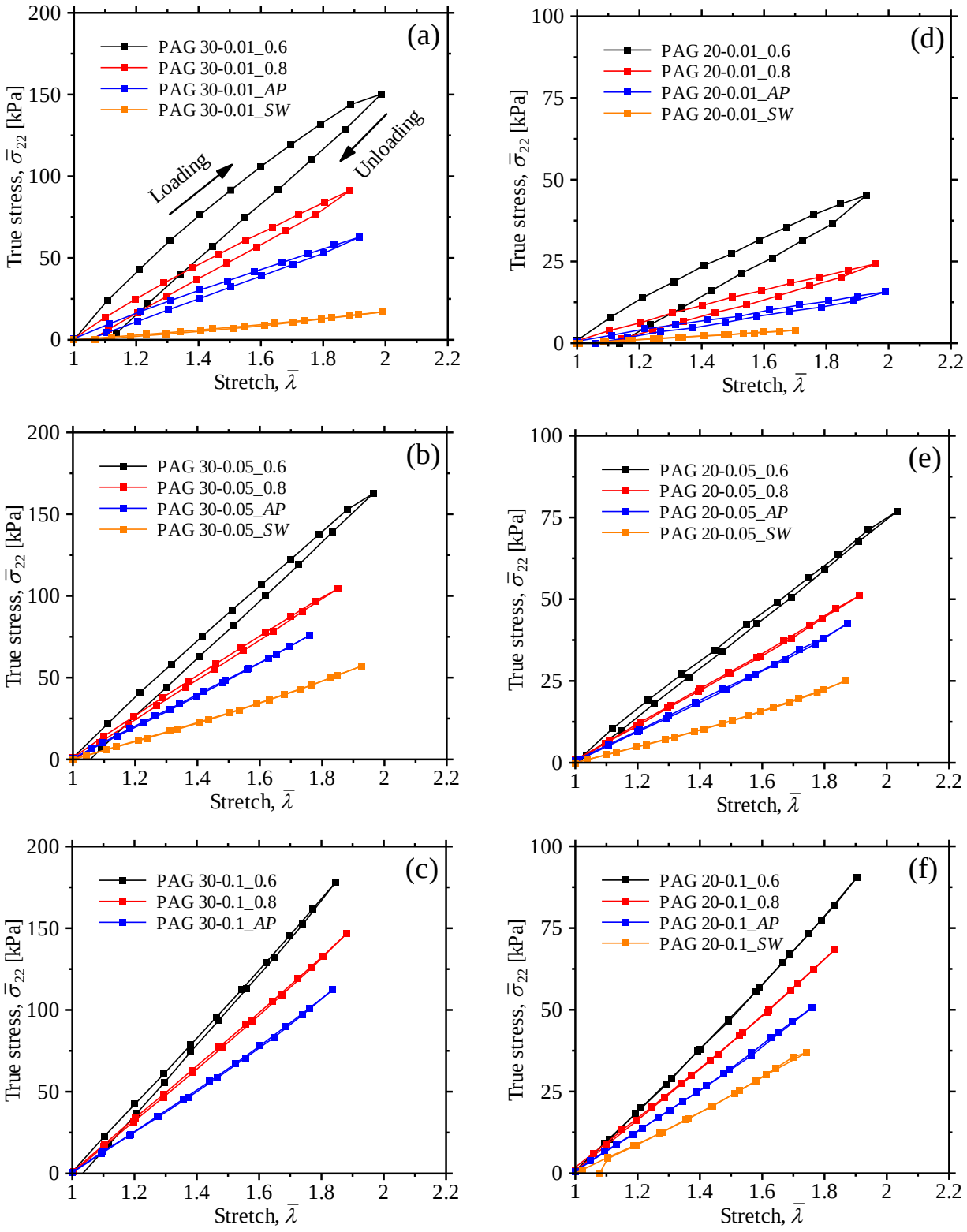

Fig. 3 Relationships between the true stress and stretch for (a) PAG $30-0.01$, (b) 0.05, (c) 0.1, (d) $20-0.01$, (e) $20-0.05$, (f) $20-0.1$. The black, red, blue, and orange lines represent models for $C^x - C^y$_0.6, 0.8, AP, and SW, respectively. Note that the scales of the vertical axes between (a)-(c) and (d)-(f) are different.

The relationship between hysteresis loss and monomer density was analyzed, as shown in Fig. 4, to quantitatively investigate the irreversible response of the hydrogel. In Fig. 4, the vertical axis represents the nondimensional hysteresis loss, which is the hysteresis loss divided by the maximum stress. The horizontal axis represents the monomer density, which is expressed by C^x/J, where C^x is the monomer density of the AP specimen, and J is the volume ratio of the swollen/dried and AP hydrogels. The solid and dashed lines represent the results for $C^x = 20$ wt% and 30 wt%, respectively. The hysteresis loss during the loading-unloading cycle increased with increasing monomer density for all hydrogel specimens prepared in this study. These results indicate that more significant intermolecular interactions occur in hydrogels with smaller intermolecular chain distances. Furthermore, the hysteresis loss decreased with increasing initial cross-linker density. Because the number of molecular chain segments should be smaller in a highly cross-linked hydrogel, chain expansion in the lateral direction is limited (detailed in the following section). This results in an increase in the distance between adjacent molecular chains.

To summarize the effect of the hydrogel composition and solvent contents on the elastic-to-inelastic transition, a phase diagram is established in Fig. 5. Vertical and horizontal axes of Fig. 5 are weight percentages of the crosslinker

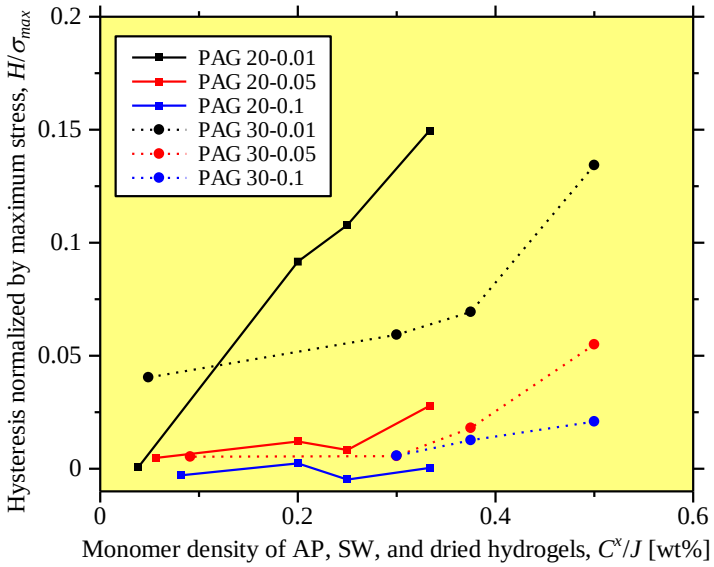

Fig. 4 Relationships between hysteresis loss and monomer density where the vertical axis represents the nondimensional hysteresis loss divided by the maximum stress, and the horizontal axis represents the monomer densities of AP, SW, and dried hydrogel specimens. The solid and dashed lines are results for $C^x = 20$ and 30 wt%, respectively.

and monomer, C_y and C_x, respectively, and the hydrogel specimen showing the elastic and inelastic responses are plotted by open square and red circle, respectively. The diagram clearly shows that the hydrogel specimens with lower C_x and higher C_y exhibit inelastic behavior. A discrete elastic-to-inelastic transition boundary is drawn in the figure. A more accurate boundary line can be provided by additional experiments with hydrogels with various compositions and solvent contents. From these experimental results, the irreversible response during the loading-unloading cycle was characterized by the initial densities of the monomer and cross-linker and the solvent contents. In the following section, a parameter corresponding to the intermolecular chain distance is introduced to describe the irreversible mechanical behavior of hydrogel based on the experimental results.

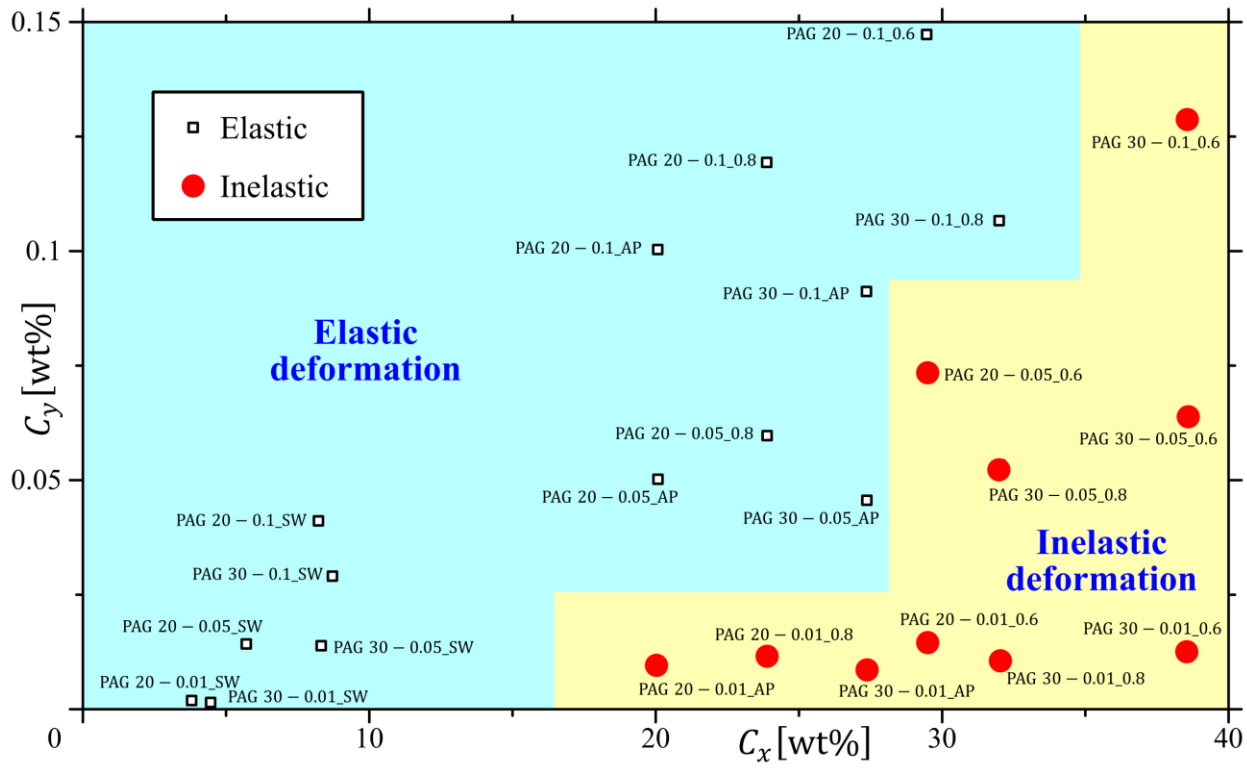

Fig. 5 Phase diagram of elastic-to-inelastic transition. Vertical and horizontal axes of Fig. 5 are weight percentages of the crosslinker and monomer, C_y and C_x, respectively, and the hydrogel specimen showing the elastic and inelastic responses are plotted by open square and red circle, respectively. A discrete elastic-to-inelastic transition boundary is drawn in the figure.

3 Constitutive modeling

3.1 Theory

A series of experimental results revealed that the loading-unloading response of the hydrogel was significantly influenced by the densities of the molecular chain, crosslink, and solvent contents. In particular, a pronounced irreversible response was observed during the loading and unloading tests for the hydrogel with a high molecular chain density and a decreasing crosslink density. This result indicated that the intermolecular interactions inducing the irreversible response increased owing to a decrease in the intermolecular chain distance. In this section, parameters characterizing the intermolecular chain distance are introduced to characterize the mechanical behaviors of the swollen and dried hydrogels.

Consider the crosslinked (CL) molecular chain network with chain density n^{CL} in the AP state. Fig. 6 shows a schematic of the change in the intermolecular chain distance during swelling and drying. An eight-chain model

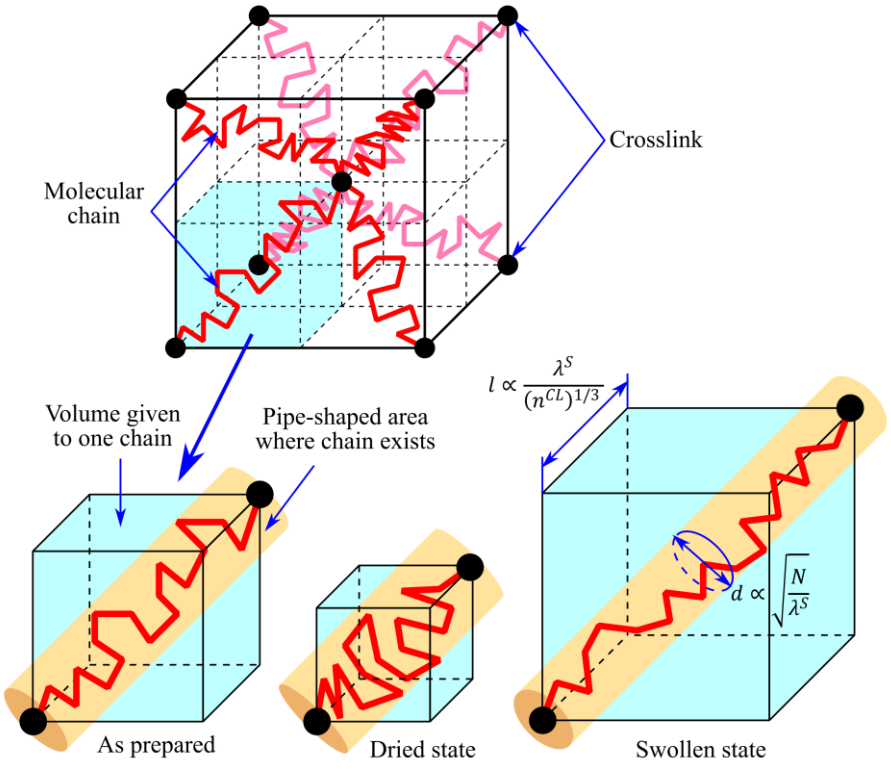

Fig. 6 Schematic of change in the intermolecular chain distance during swelling and drying. Volume given to one chain is represented by the light-blue cube, whereas the pipe-shaped area where the chain exists is depicted by the light-brown pipe.

[Arruda and Boyce, 1993] was depicted as a reference image representing the molecular chain network. The volume of one molecular chain, which is depicted by the light-blue cube in Fig. 6, for the AP hydrogel with a crosslink density of n^{CL} is $1/n^{CL}$. If the volume of the hydrogel changes by swelling or drying from V_0 to V, the volume of one chain is expressed by J/n^{CL}, where $J = V/V_0$. Because the chain stretching λ^S accompanied by the volume change is isotropic, $J = (\lambda^S)^3$. Therefore, the length of this volume depends on $\lambda^S/(n^{CL})^{1/3}$.

In contrast, the volume in which the molecular chain exists does not coincide with the volume of one chain. In this study, we assumed that the molecular chain extended inside the pipe-shaped space, as illustrated by the light-brown pipe in Fig. 6. In the random-walk molecular chain model, the average distance between both edges of the molecular chain on which the segments rotate randomly is expressed by $\sqrt{N}l^S$, where N is the number of segments in a chain, and l^S is the length of each segment [38]. If that the random segments spread isotropically in a zero-stress state, the pipe diameter should be proportional to $\sqrt{N}l^S$. When chain stretch λ^S is caused by swelling or drying, the decreased pipe diameter is proportional to $\sqrt{N/\lambda^S}l^S$. Therefore, the intermolecular chain distance in a specific direction is assumed to be proportional to $\lambda^S/(n^{CL})^{1/3}$ and $-\sqrt{N/\lambda^S}l^S$. The volume of the pipe is assumed to remain constant. Considering that l^S is the constant, we introduced the following nondimensional parameter ϕ corresponding to the intermolecular chain distance:

$$\phi = C_1 \frac{\lambda^S}{(n^{CL})^{1/3}} - C_2 \sqrt{\frac{N}{\lambda^S}} \tag{7}$$

where C_1 and C_2 are positive constants, such that ϕ ranges from 0 to 1.

When $\phi = 0$, the intermolecular chain distance is sufficiently small to generate an intermolecular interaction, which behaves as intermolecular bonding, whereas $\phi = 1$ represents no intermolecular interaction. This bonding due to the intermolecular interaction is referred to as the secondary bond (SB), which is weaker than that caused by cross-linking and physical entanglement. Because a three-dimensional network is formed through intermolecular interaction, the SB chain density, n^{SB}, should be proportional to $(1-\phi)^3$. Consequently, the ratios of the densities of the CL and SB chains are expressed as follows:

$$\begin{cases} \dfrac{n_0^{SB}}{n^{CL}} = 0 & (\phi > 1) \\ \dfrac{n_0^{SB}}{n^{CL}} = C_3(1-\phi)^3 & (0 \le \phi \le 1) \\ \dfrac{n_0^{SB}}{n^{CL}} = C_3 & (\phi < 0) \end{cases} \tag{8}$$

where C_3 is constant.

The number of segments in a chain decreased with an increasing SB density. As the total number of segments of the polymer is constant, the number of segments per chain is expressed as follows:

$$N = \frac{n^{CL}}{n^{CL} + n_0^{SB}} N_0 \tag{9}$$

where N_0 is the number of segments per chain for the $n_0^{SB} = 0$ case.

Subsequently, a visco-hyperelastic mechanical model was established by introducing the SB density evaluated using ϕ into the TN theory. Uchida et al. proposed a viscoelastic-viscoplastic TN model to represent the time- and temperature-dependent mechanical behaviors of glassy and semi-crystalline polymers [Uchida et al., 2019b, 2022, 2024; Yoshida et al., 2022]. In their proposed model, few assumption were made, namely, (i) the molecular chain network is assumed to be constructed by strongly fixed CL and debondable SBs, and (ii) the debonding and rebonding of SB is related to the nonlinear mechanical behavior of the polymer. The basic concept model is a parallel mechanical system consisting of CL and SB molecular chain networks as shown in Fig. 7. An entropic elasticity spring was

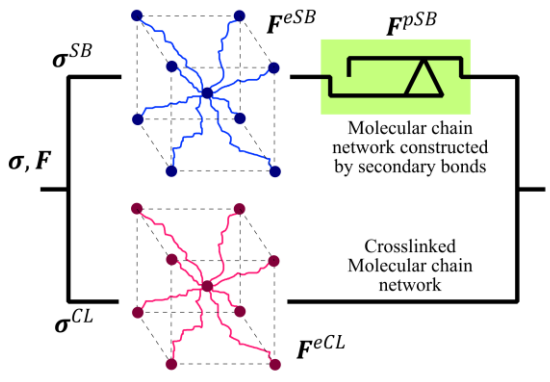

Fig. 7 Parallel mechanical system consisting of CL and SB molecular chain networks [Uchida et al., 2019b, 2022]. The entropic elasticity spring is allocated at the CL line, whereas the entropic elasticity spring and inelastic slider are given to the SB line.

assigned to the CL line to describe the reversible response of the crosslinked network of the hydrogel. In contrast, an entropic elasticity spring and inelastic slider were applied to the SB line to describe the irreversible response induced by debonding and rebonding of the SBs. The equilibrium and compatibility of this system can be expressed as follows:

$$\begin{aligned} \boldsymbol{\sigma} &= \boldsymbol{\sigma}^{CL} + \boldsymbol{\sigma}^{SB} \\ \boldsymbol{F} &= \boldsymbol{F}^{eCL} = \boldsymbol{F}^{eSB}\boldsymbol{F}^{pSB} \end{aligned} \tag{10}$$

where $\boldsymbol{\sigma}$, and $\boldsymbol{F}$ are Cauchy stress and deformation gradient for the entire system. $\boldsymbol{\sigma}^{CL}$ and $\boldsymbol{\sigma}^{SB}$ are the Cauchy stresses for the CL and SB springs, which are related to elastic deformation gradients $\boldsymbol{F}^{eCL}$ and $\boldsymbol{F}^{eSB}$, respectively. Further, $\boldsymbol{F}^{CL}$ and $\boldsymbol{F}^{eSB}$ are related to the stretching of molecular chains, whereas $\boldsymbol{F}^{pSB}$ is related to the intermolecular slip during the debonding and rebonding.

For the constitutive equation of the springs, the classical Arruda-Boyce mode [Arruda and Boyce, 1993] was employed as follows:

$$\boldsymbol{\sigma}^{\Pi} = \frac{1}{3} C^{R\Pi} \frac{\sqrt{N}}{\lambda_c^{e\Pi}} \Lambda^{-1}\left(\frac{\lambda_c^{e\Pi}}{\sqrt{N}}\right)\{\boldsymbol{A}^{e\Pi} - (\lambda_c^{e\Pi})^2\boldsymbol{I}\} - p^{\Pi}\boldsymbol{I} \qquad (\Pi = \text{CL or SB}) \tag{11}$$

where $C^R = n\kappa_B T$ is the rubbery elasticity, n is the molecular chain density, κ_B is the Boltzmann's constant, T is the absolute temperature, $\boldsymbol{A}^e = \boldsymbol{F}^e(\boldsymbol{F}^e)^T$ is the left Cauchy-Green deformation tensor, $\lambda_c^e = \mathrm{tr}(\boldsymbol{A}^e)/3$ is the chain stretch, $\boldsymbol{I}$ is the second-order unite tensor, $\Lambda^{-1}(x)$ is the inverse of the Langevin function $\Lambda(x) = \coth x - 1/x$, and p is the hydrostatic pressure to impose the incompressibility constant. This model enables the prediction of the swelling limit of gels because the critical stretch owing to the orientation of the molecular chain is introduced [Okumura and Chester, 2018].

Elastic deformation gradient $\boldsymbol{F}^{e\Pi}$ can be further decomposed into gradients by external loading and swelling/drying, $\boldsymbol{F}^{el\Pi}$ and $\boldsymbol{F}^{ev\Pi}$, respectively. As the change in volume owing to swelling and drying is isotropic, that is, $\boldsymbol{F}^{ev\Pi} = \lambda_c^{ev\Pi}\boldsymbol{I}$, Eq. (11) can be rewritten as follows [Uchida et al., 2019a].

$$\boldsymbol{\sigma}^{\Pi} = \frac{1}{3}\frac{C^{R\Pi}}{\left(\lambda_c^{ev\Pi}\right)^3}\frac{\sqrt{N}/\lambda_c^{ev\Pi}}{\lambda_c^{el\Pi}}\Lambda^{-1}\left(\frac{\lambda_c^{el\Pi}}{\sqrt{N}/\lambda_c^{ev\Pi}}\right)(\lambda_c^{ev\Pi})^2\{\boldsymbol{A}^{el\Pi} - (\lambda_c^{el\Pi})^2\boldsymbol{I}\} - p^{\Pi}\boldsymbol{I} \tag{12}$$

$$= \frac{1}{3}\frac{C^{R\Pi}}{\lambda_c^{ev\Pi}}\frac{\sqrt{N}/\lambda_c^{ev\Pi}}{\lambda_c^{el\Pi}}\Lambda^{-1}\left(\frac{\lambda_c^{el\Pi}}{\sqrt{N}/\lambda_c^{ev\Pi}}\right)\{\boldsymbol{A}^{el\Pi} - (\lambda_c^{el\Pi})^2\boldsymbol{I}\} - p^{\Pi}\boldsymbol{I}$$

Pressure in the network can be expressed as follows:

$$p^{\Pi} = -\psi^{\Pi}(\ln J^{el\Pi} + \ln J^{ev\Pi}) \tag{13}$$

where ψ is the bulk modulus, $J^e = \det(\boldsymbol{F}^e)$. Because the pressure induced by swelling and drying should balance with the osmotic pressure of the solvent, $\boldsymbol{F}^{eV}$ does not perform any work under external loading without solvent transfer. Therefore, Eq. (12) for the tensile test can be expressed as follows.

$$\boldsymbol{\sigma}^{\Pi} = \frac{1}{3}\frac{C^{R\Pi}}{\lambda_c^{ev\Pi}}\frac{\sqrt{N}/\lambda_c^{ev\Pi}}{\lambda_c^{el\Pi}}\Lambda^{-1}\left(\frac{\lambda_c^{el\Pi}}{\sqrt{N}/\lambda_c^{ev\Pi}}\right)\{\boldsymbol{A}^{el\Pi} - (\lambda_c^{el\Pi})^2\boldsymbol{I}\} + \psi^{\Pi}\ln J^{el\Pi}\boldsymbol{I} \tag{14}$$

In the original TN model proposed for the viscoelastic behavior of rubber, the intermolecular chain bonding was categorized by the permanent crosslink and transient slippage link, and the free energy is estimated based on the statistical approach [Tanaka and Edward, 1992; Vernerey et al., 2017; Sridhar and Vernerey, 2020]. In contrast, Uchida et al. (2019) proposed the VE-VP TN theory, in which the density of the molecular chain bonded by SB decreases and increases depending on applied stress and remaining SB density. In this model, the development equations of chain density were represented by a specific rate form. This enabled the representation of the nonlinear viscoelastic response before the yielding and the stress decrease after yielding in the glassy polymer [Uchida et al., 2019b, 2022] and semi-crystalline polymer [Yoshida et al., 2022; Uchida et al., 2024]. In the TN model, the specific rates of debonding and rebonding, the specific debonding and rebonding rates are expressed as follows [Uchida et al., 2019b, 2022]:

$$\dot{r}^{(-)} = \dot{r}_0^{(-)}\frac{n^{SB}(t)}{n_0^{SB}}\left(\frac{\sigma_{eq}^{SB}}{\sigma_0}\right)^{\alpha} \tag{15}$$

$$\dot{r}^{(+)} = \dot{r}_0^{(+)}\left(1 - \frac{n^{SB}(t)}{n_0^{SB}}\right) \tag{16}$$

where $\dot{r}_0^{(-)}$ and $\dot{r}_0^{(+)}$ are the reference specific rates for debonding and rebonding, respectively, n_0^{SB} and $n^{SB}(t)$ are the initial and current SB densities, respectively, σ_{eq}^{SB} is the equivalent stress for the SB network, σ_0 is the resistance to debonding, and α is the stress sensitivity. The total rate of change in the SB density was obtained using $\dot{r}^{(-)}$ and $\dot{r}^{(+)}$ as follows:

$$\dot{n}^{SB} = n_0^{SB}\left(-\dot{r}^{(-)} + \dot{r}^{(+)}\right) \tag{17}$$

Furthermore, the rate of change in the number of segments is expressed as follows.

$$\dot{N} = -\frac{\dot{n}^{\Pi}}{n_0^{\Pi}} N_0 \tag{18}$$

The magnitude of the intermolecular flow is represented by the rebonding of the debonded site as follows:

$$\dot{\varepsilon}^{pSB} = b\dot{r}^{(+)} \tag{19}$$

where b is a constant. By obeying the flow rule in the viscoelastic-viscoplastic TN model, the velocity gradient for the inelastic slider, $\boldsymbol{L}^{pSB} = \dot{\boldsymbol{F}}^{pSB}(\boldsymbol{F}^{pSB})^{-1}$, is expressed as follows.

$$\boldsymbol{L}^{pSB} = \dot{\varepsilon}^{pSB}(\boldsymbol{F}^{elSB} - \boldsymbol{I}) \tag{20}$$

The detailed formulation process is provided in references [Uchida et al., 2019b, 2022]. The thermodynamic consistency of the proposed model is presented in Appendix A.

3.2 Simulation results

Using the proposed model, we performed numerical simulations of the loading and unloading uniaxial tensile tests in the x_2 direction under the same conditions as described in the experimental section. As shown in Fig. 2, the strain field on the specimen was almost uniform. Therefore, the mechanical response under the uniform stress state is directly solved using Eqs. (14) in the time-incremental calculation with the following boundary conditions:

$$\dot{\boldsymbol{F}} = \begin{bmatrix} \text{unknown} & 0 & 0 \\ 0 & \dot{U}/L_0 & 0 \\ 0 & 0 & \text{unknown} \end{bmatrix} \tag{21}$$

$$\boldsymbol{\sigma} = \begin{bmatrix} 0 & 0 & 0 \\ 0 & \text{unknown} & 0 \\ 0 & 0 & 0 \end{bmatrix} \tag{22}$$

where $\dot{U}$ is the constant tensile velocity. This boundary problem was solved by an in-house code. First of each time-incremental step, a tentative deformation gradient rate $\dot{\boldsymbol{F}}$ including undefined unknown component was given to the Eq. (14). The stress tensor $\boldsymbol{\sigma}$ calculated using tentative $\dot{\boldsymbol{F}}$ was compared with the stress boundary condition Eq. (22). $\dot{\boldsymbol{F}}$ was renewed to decrease the difference in the stress components between calculated and known boundary values using the stiffness matrix in the rate-form constitutive equation, which is presented in the reference [Uchida

et al., 2019; 2022]. This calculation was repeated until the difference in the modification of $\dot{\boldsymbol{F}}$ became small.

The material parameters used in the proposed model were n^{CL}, N_0, C_1, C_2. C_3, $\dot{r}_0^{(-)}$, $\dot{r}_0^{(+)}$, σ_0, α, b, and ψ^{Π}. Due to the tensile stretch in the x_2 direction, $\sigma_{11} = \sigma_{33} = 0$, which result in Eq. (23) as

$$\sigma_{22} = \sigma_{22} - \sigma_{11} = \sigma_{22}^{CL\prime} + \sigma_{22}^{SB\prime} - \sigma_{11}^{CL\prime} - \sigma_{11}^{SB\prime} \tag{23}$$

where $\boldsymbol{\sigma}^{\Pi\prime} = \boldsymbol{\sigma}^{\Pi} - \psi^{\Pi}\ln(J^{el\Pi})\boldsymbol{I}$ is the deviatoric part of $\boldsymbol{\sigma}^{\Pi}$. Therefore, bulk modulus ψ^{Π} was omitted from the parameter-fitting process. The remaining parameters were divided into respective and common parameter sets, $\boldsymbol{q}_1(I_G) = \left(n^{CL}(I_G), N_0(I_G)\right)^T$, where I_G is the specimen name (PAG$20-0.01$ to PAG$30-0.1$), and $\boldsymbol{q}_2 = \left(C_1, C_2, C_3, \dot{r}_0^{(-)}, \dot{r}_0^{(+)}, \sigma_0, \alpha, b\right)^T$, respectively. $\boldsymbol{q}_1(I_G)$ was separately fitted for every hydrogel composition by referring to results for different solvent contents, AP, SW, 0.8, and 0.6, whereas the common parameter set, $\boldsymbol{q}_2$, was fitted using all experimental data.

To obtain the parameter sets $\boldsymbol{q}_1(I_G)$ and $\boldsymbol{q}_2$, the following error functions $\Phi_1(I_G)$ and Φ_2 were introduced:

$$\Phi_1(I_G) = \sum_{I_S=1}^{N_S}\sum_{I_\varepsilon=1}^{N_\varepsilon}\left\{\sigma^{Exp}(I_G, I_S, I_\varepsilon) - \sigma^{Sim}(I_G, I_S, I_\varepsilon, \boldsymbol{q}_1(I_G), \boldsymbol{q}_2)\right\}^2 \tag{24}$$

$$\Phi_2 = \sum_{I_G=1}^{N_G}\sum_{I_S=1}^{N_S}\sum_{I_\varepsilon=1}^{N_\varepsilon}\left\{\sigma^{Exp}(I_G, I_S, I_\varepsilon) - \sigma^{Sim}(I_G, I_S, I_\varepsilon, \boldsymbol{q}_1(I_G), \boldsymbol{q}_2)\right\}^2 \tag{25}$$

where σ^{Exp} and σ^{Sim} are the tensile nominal stresses obtained from the experiment and simulation, N_G, N_S, and N_ε are the numbers of hydrogel composition patterns, solvent contents patterns, and stress-strain plots. Parameter sets $\boldsymbol{q}_1(I_G)$ and $\boldsymbol{q}_2$ were fitted using the nonlinear least-squares method made in-house. The flowchart of the parameter fitting is shown in Fig. 8. First, the initial tentative parameter sets $\boldsymbol{q}_1^{(0)}(I_G)$ and $\boldsymbol{q}_2^{(0)}$ were prepared. Subsequently, $\boldsymbol{q}_1^{(1)}(I_G)$ for the I_Gth gel specimen was fitted by solving the following equation with the initial tentative $\boldsymbol{q}_2$:

$$\frac{\partial\Phi_1(I_G)}{\partial\boldsymbol{q}_1(I_G)} = \sum_{I_S=1}^{N_S}\sum_{I_\varepsilon=1}^{N_\varepsilon}\left\{\sigma^{Exp}(I_G, I_S, I_\varepsilon) - \sigma^{Sim}(I_G, I_S, I_\varepsilon, \boldsymbol{q}_1(I_G), \boldsymbol{q}_2)\right\}\frac{\partial\sigma^{Sim}}{\partial\boldsymbol{q}_1(I_G)} = \boldsymbol{0} \tag{26}$$

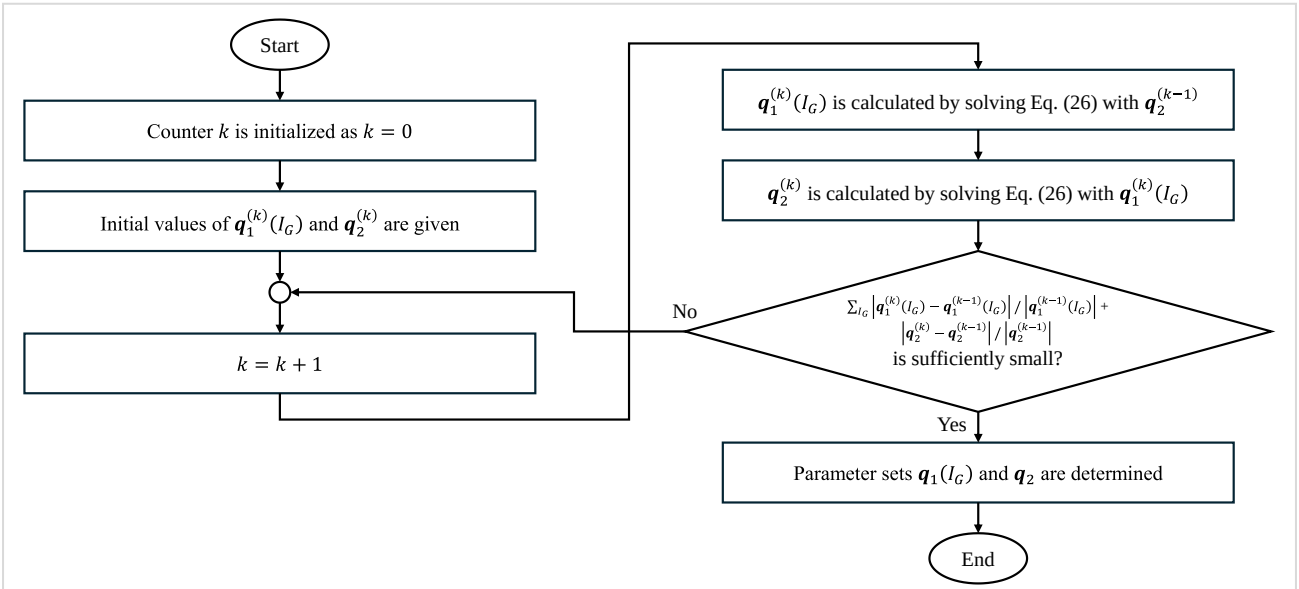

Fig. 8 Flowchart of the fitting process of material parameter set $\boldsymbol{q}_1(I_G)$ and $\boldsymbol{q}_2$. Parameter sets are alternately updated using Eqs. (26) and (27) for every iteration step k. The nonlinear simultaneous equations (26) and (27) were solved by the Newton-Raphson iterative scheme.

Using obtained $\boldsymbol{q}_1^{(1)}(I_G)$, $\boldsymbol{q}_2^{(1)}$ was obtained by solving the following equation:

$$\frac{\partial \Phi_2}{\partial \boldsymbol{q}_2} = \sum_{I_G=1}^{N_G}\sum_{I_S=1}^{N_S}\sum_{I_\varepsilon=1}^{N_\varepsilon}\left\{\sigma^{Exp}(I_G, I_S, I_\varepsilon) - \sigma^{Sim}(I_G, I_S, I_\varepsilon, \boldsymbol{q}_1(I_G), \boldsymbol{q}_2)\right\}\frac{\partial \sigma^{Sim}}{\partial \boldsymbol{q}_2} = \boldsymbol{0} \qquad (27)$$

The nonlinear simultaneous equations (26) and (27) were solved by the Newton-Raphson iterative scheme. Using updated $\boldsymbol{q}_2^{(1)}$, we obtain $\boldsymbol{q}_1^{(2)}(I_G)$ by Eq. (26). This process was repeated until the change in the parameter sets $\boldsymbol{q}_1(I_G)$ and $\boldsymbol{q}_2$ became small.

The fitted parameters listed in Tables 2 and 3 and the plotted stress-strain curves for all conditions are shown in Fig. 8. In Fig. 8, the experimental results are plotted using marks, and the simulation results are plotted as solid lines. As shown in Fig. 9, the proposed model reasonably reproduces the experimental results. Although the stress difference in hydrogels with different solvent contents was underestimated in a previous study [Uchida et al, 2019a], introduction of the intermolecular interactions appropriately reproduced the experimentally evaluated mechanical responses. Furthermore, the proposed model could quantitatively and qualitatively represent the critical characteristics of dried hydrogels, in which the irreversible response was increased by increasing the molecular chain density and decreasing the cross-linking density.

Table 2 Respective parameters

	PAG $20-0.01$	PAG $20-0.05$	PAG $20-0.1$	PAG $30-0.01$	PAG $30-0.05$	PAG $30-0.1$
$n^{CL}\kappa_B T$ [kPa]	2.47	13.49	17.1	9.69	22.71	27.37
N $[-]$	191.2	14.4	5.78	67.0	9.10	6.46

Table 3 Common parameters

$C_1[\mathrm{nm}^{-1}]$	$C_2[-]$	$C_3[-]$	$\dot{r}_0^{(-)}\,[s^{-1}]$	$\dot{r}_0^{(+)}\,[s^{-1}]$	σ_0 [kPa]	α $[-]$	b $[-]$
0.1155	0.108	5.25	0.019	0.0016	1020.5	0.2659	2.35

The above results revealed that the inelastic nature of the mechanical response of the hydrogel could be characterized by intermolecular interaction. In other words, the magnitude of the intermolecular interaction of the hydrogel may be quantified by evaluating the irreversibility of the mechanical response. As an example of quantifying the irreversibility of the mechanical response, the relationship between hysteresis loss from the loading to unloading cycle and the parameter ϕ introduced in this study was evaluated. The nondimensional hysteresis loss H/σ_{max} against $(1-\phi)^3$ was plotted (Fig. 9). The black and red markers represent the experimental and simulation results, respectively, and the shape of the marker represents the hydrogel composition. Although the monomer density, which is the horizontal axis of Fig. 4, cannot represent the hysteresis loss for hydrogels with different compositions, it can be plotted around the unified curves when the horizontal axis is $(1-\phi)^3$. Therefore, ϕ is an appropriate parameter for quantifying the intermolecular interaction of the hydrogels.

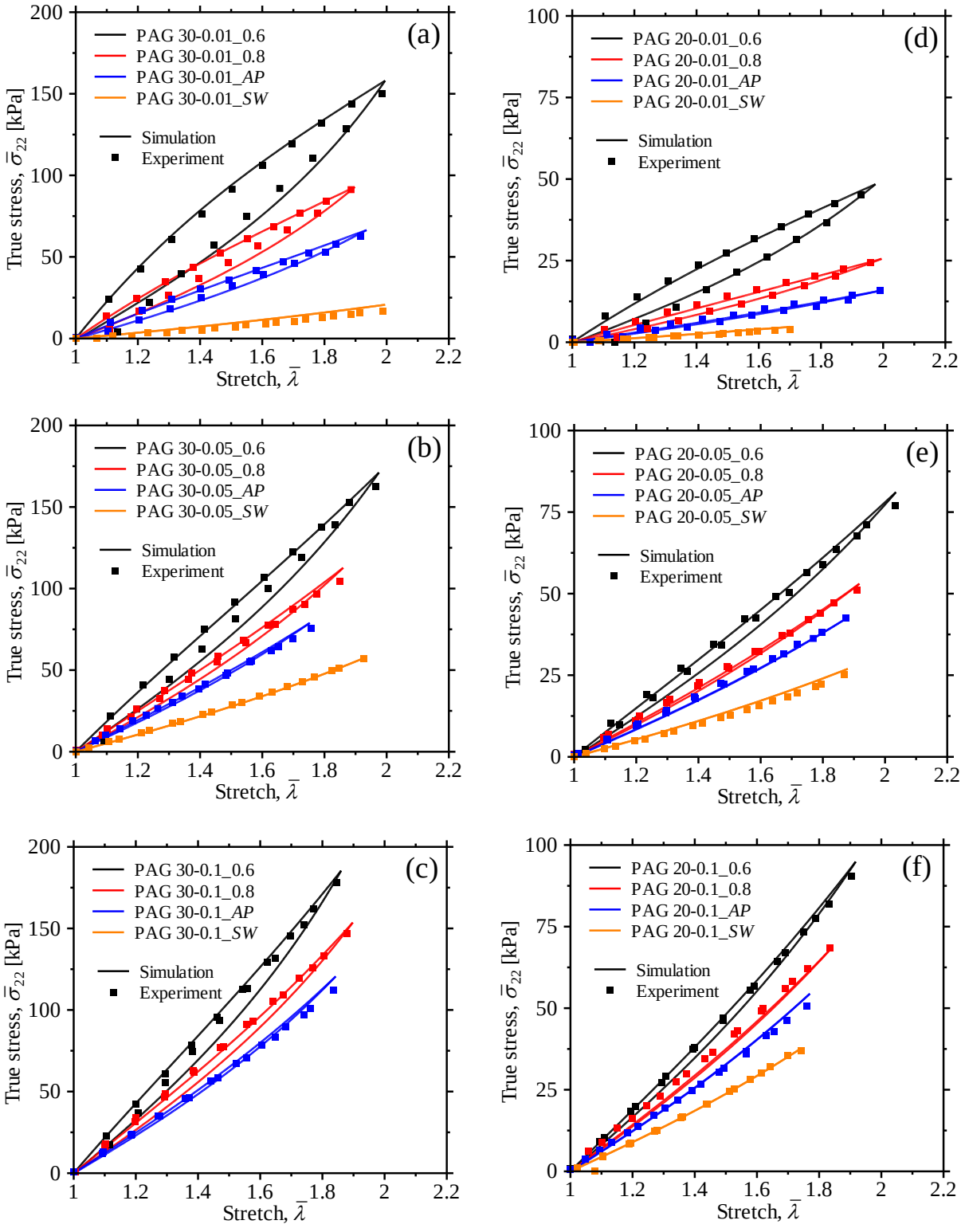

Fig. 9 Relationships between the true stress and the stretch for (a) PAG $30-0.01$, (b) 0.05, (c) 0.1, (d) $20-0.01$, (e) $20-0.05$, and (f) $20-0.1$. The experimental results are represented by marks, whereas the simulation results are represented by solid lines.

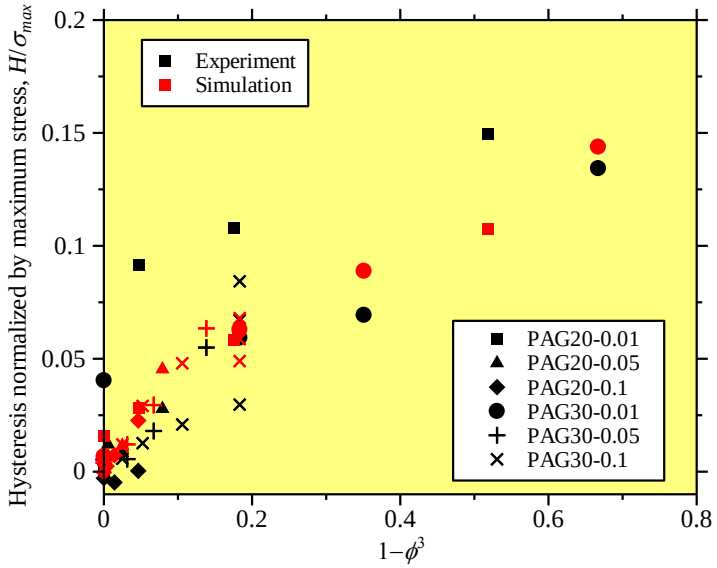

Fig. 10 Relationships between hysteresis and $(1-\phi)^3$. ϕ is a nondimensional parameter obtained using Eq. (7), which represents the intermolecular chain distance. The hysteresis loss for all the hydrogel specimens with different monomer and cross-linker densities and solvent content can be obtained using ϕ.

1

2 3.3 Discussion

3 We established the visco-hyperelastic transient network model, in which the parameter corresponding to the
4 intermolecular-chain distance was introduced. The irreversible mechanical responses of hydrogels with different
5 compositions and solvent contents under the uniaxial tensile loading-unloading tests were successfully represented
6 by the model. In this section, several issues regarding the proposed model, i.e., parameter relationship, application
7 for time-dependent behavior, and further improvement, are discussed.

8 In this model, parameters $n^{CL}\kappa_B T$ and N were independently determined for each hydrogel composition.
9 Therefore, additional experiments are required to predict the inelastic behavior of hydrogels with new compositions.
10 Here, the evolution laws of parameters $n^{CL}\kappa_B T$ and N are discussed using the hydrogel composition listed in Table
11 1. The change in the fitted $n^{CL}\kappa_B T$ and N are plotted as a function of the weight ratios of monomer C_x and
12 crosslinker C_y in Fig. 11. In Fig. 11, left and right vertical axes are $n^{CL}\kappa_B T$ and N, which are plotted by open
13 squares and filled circles, respectively, horizontal axis is C_y, color of marks corresponds to C_x. With the increase in

the weight ratios of monomer and crosslinker, $n^{CL}\kappa_B T$ and N nonlinearly increases and decreases, respectively, similar to the previous study [Uchida et al., 2019]. These changes in $n^{CL}\kappa_B T$ and N with the hydrogel composition C_x and C_y were represented by the following simple evolution laws:

$$n^{CL}\kappa_B T = (f_1 + f_2 C_x) C_y^{f_3} \tag{28}$$

$$N = (g_1 + g_2 C_x) C_y^{g_3} \tag{29}$$

Table 4 Parameters in the evolution laws of $n^{CL}\kappa_B T$ and N

f_1 [kPa]	f_2 [kPa]	f_3 [−]	g_1 [−]	g_2 [−]	g_3 [−]
−29.7	4.09	0.473	0.904	−0.0229	−1.24

The constants f_1 to f_2 and g_1 to g_2 obtained from the least square method are listed in Table 4, and the Eqs. (28) and (29) are plotted in Fig. 11. Although sufficient experimental data were not provided in the present study, these equations reasonably represent the nonlinear increase and decrease in $n^{CL}\kappa_B T$ and N. Accumulation of experimental data of hydrogels with new compositions and solvent contents improves the accuracy of representations

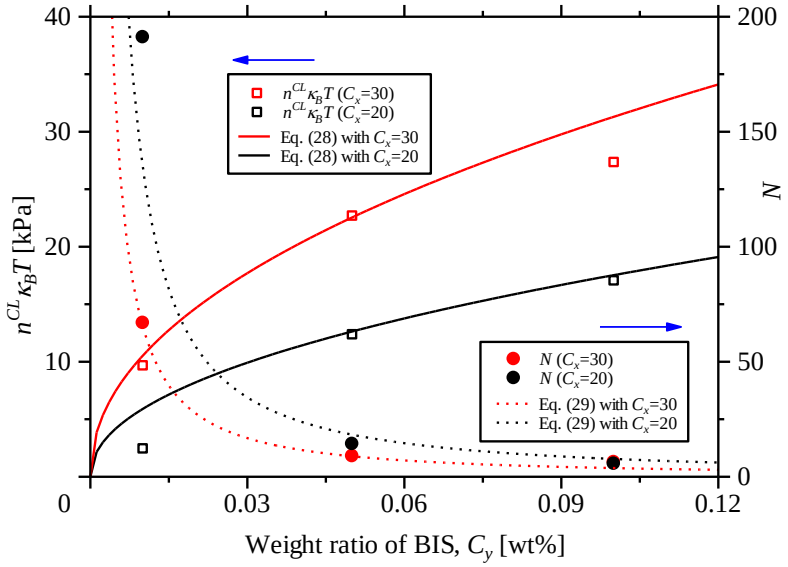

Fig. 11 Relationships between $n^{CL}\kappa_B T$ and N and the weight ratios of monomer C_x and crosslinker, C_y. Left and Right vertical axes are $n^{CL}\kappa_B T$ and N, which are plotted by open squares and filled circles, respectively, horizontal axis is C_y, color of marks and line correspond to C_x.

of these parameters. It enables prediction of the inelastic behavior of arbitrary hydrogels.

Subsequently, the proposed model is applied to predict the time-dependent mechanical behavior of hydrogel specimens. Fig. 12 shows the relationships between true stress and stretch under the uniaxial tensile loading-unloading tests with different displacement rates, 8, 20, and 30 mm/min. (a) and (b) are experimental and simulation results, respectively. PAG30 − 0.01_AP was used in this experiment. The proposed model could predict the increase in the slope of the stress-stretch curve with tensile displacement rate and hysteresis loss during the loading-unloading cycle. However, the magnitudes of hysteresis loss depended on the strain rate in the experimental results, whereas those obtained from the simulation were almost independent of the strain rate. Furthermore, the model underestimated the residual stretch after the unloading. To improve the accuracy for predicting the time-dependent hysteresis loss and residual stretch, further extensions of the evolution laws for the debonding and rebonding rates and inelastic strain rate in the TN theory will be studied based on the experimental results of the loading-unloading responses with different strain rates.

In addition to the above, several potential extensions of the model are discussed. The time-dependent behavior of hydrogel is characterized by not only the mechanical property but also the chemical phenomenon, such as diffusion,

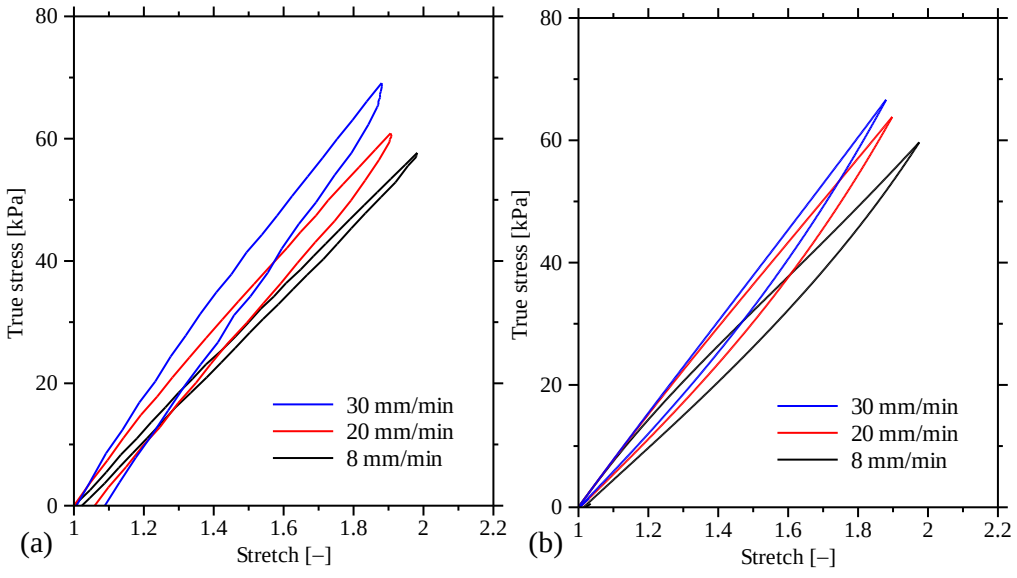

Fig. 11 Relationships between true stress and stretch under uniaxial tensile loading-unloading tests with different displacement rate, 8, 20, and 30 mm/min. (a) and (b) are experimental and simulation results, respectively. PAG30 − 0.01_AP was used in this experiment.

swelling, and evaporation of the solvent. The introduction of the mechanochemical coupling model is important to predict the strength and flexibility of the biomedical materials and soft actuators. Furthermore, the deformation range employed in this study (a maximum stretch of 1.75) is relatively smaller because the hydrogel showed stretch of $\lambda > 10$ depending on its composition. The large strain range of polymer deformation is characterized by significant hardening owing to the orientation of the molecular chain in the elongation direction. The present study should be extended to elucidate the inelastic deformation in such a large strain range for further understanding of the intermolecular chain interaction of the polymer.

Appendix A: Thermodynamic consistency

In the isothermal case, the Clausius-Duhem inequality is given as follows [Holzapfel, 2000; Anssari-Benam and Zaïri, 2024a, 2024b, 2025]:

$$\frac{1}{2}\boldsymbol{\sigma}:\Delta\boldsymbol{A}-\Delta\psi\geq 0 \tag{A1}$$

where $\Delta\psi$ is change in the free energy. In this study, the concrete form of free energy is not provided. Because the stress given by Eq. (14) is a function of the left Cauchy-Green deformation tensor $\boldsymbol{A}$ and the chain density n, the change in the free energy can be estimated as follows:

$$\Delta\psi=\frac{1}{2}\frac{\partial(\boldsymbol{\sigma}:\Delta\boldsymbol{A})}{\partial\Delta\boldsymbol{A}}:\Delta\boldsymbol{A}+\frac{1}{2}\frac{\partial(\boldsymbol{\sigma}:\Delta\boldsymbol{A})}{\partial n}\Delta n=\frac{1}{2}\boldsymbol{\sigma}:\Delta\boldsymbol{A}+\frac{1}{2}\frac{\partial\boldsymbol{\sigma}}{\partial n}:\Delta\boldsymbol{A}\Delta n \tag{A2}$$

Substituting Eq. (A2) into Eq. (A2), we obtain

$$\frac{1}{2}\frac{\partial\boldsymbol{\sigma}}{\partial n}:\Delta\boldsymbol{A}\Delta n\leq 0 \tag{A3}$$

Parameters changing with n in Eq. (14) are C^R, $\sqrt{N}$, and $\Lambda^{-1}\left(\lambda_c/\sqrt{N}\right)=\beta$. Those differential forms by n are given as follows:

$$\frac{\partial C^R}{\partial n}=\kappa^B T$$

$$\frac{\partial\left(\sqrt{N}\right)}{\partial n}=-\frac{N}{2n\sqrt{N}}$$

$$\frac{\partial \beta}{\partial n} = \frac{\lambda_c}{2n\sqrt{N}} \frac{\beta^2}{1 - \beta^2 \operatorname{csch}^2 \beta} = \frac{\lambda_c}{2n\sqrt{N}} \zeta$$

Therefore, Eq. (A3) is rewritten as

$$\frac{1}{4n}\left(1 + \frac{\lambda_c \zeta}{\beta\sqrt{N}}\right)(\boldsymbol{\sigma}: \Delta \boldsymbol{A})\Delta n \leq 0 \tag{A4}$$

The terms $\left\{1 + \left(\lambda_C \zeta / \beta\sqrt{N}\right)\right\}/(4n)$ and $\boldsymbol{\sigma}: \Delta \boldsymbol{A}$ are always positive, whereas $\Delta n = n - n_0$ is always negative because initial chain density n_0 is the maximum value of n. Therefore, the Clausius-Duhem inequality is satisfied.

Conclusion

Uniaxial tensile loading-unloading tests were performed on hydrogel specimens with different densities of monomers, cross-linkers, and solvent to quantitatively evaluate the inelastic deformation induced by the intermolecular interaction. The development of the strain field during the test was measured using DIC, and the relationship between the true stress and true strain was evaluated using the obtained strain field. The stiffness and maximum stress increased with increasing monomer and cross-linker densities and decreasing solvent content. A significant difference between the loading and unloading responses was observed for the dried hydrogel specimens. Intermolecular interactions induce irreversible deformation when the intermolecular chain distance is smaller.

A non-dimensional parameter corresponding to the intermolecular chain distance was introduced to describe the irreversible response of the hydrogel observed in the experimental study. This parameter is a function of the densities of the molecular chain, number of segments per chain, and stretching accompanied by swelling and drying. Subsequently, a visco-hyperelastic model was established by introducing the proposed parameter into transient network theory. Using the established mechanical model, we performed numerical simulations of uniaxial tensile loading-unloading tests under the same conditions as in the experimental study. The simulation results qualitatively and quantitatively reproduced the experimentally observed characteristics of the mechanical response of the hydrogel. The hysteresis loss during the loading-unloading cycle was plotted around the unified function of the proposed intermolecular chain distance parameter. However, the deformation range employed in this study is relatively smaller

as compared to the hydrogel showing significantly high stretch. The large strain range of polymer deformation is characterized by significant hardening owing to the orientation of the molecular chain in the elongation direction. In addition, the present model could not represent the time-dependent hysteresis observed in the uniaxial tensile loading-unloading tests with different strain rates. The present study should be extended to elucidate the inelastic deformation in such a large strain range for further understanding of the intermolecular chain interaction of the polymer.

References

Ajam, A., Huang, Y., Islam, M. S., Kilian, K. A., Kruzic, J. J., "Mechanical and biological behavior of double network hydrogels reinforced with alginate versus gellan gum", Journal of the Mechanical Behavior of Biomedical Materials, Vol. 157 (2024), 106642.
https://doi.org/ 10.1016/j.jmbbm.2024.106642

Alkhoury, K., Ivko, R., Hossain, M., Nadimpalli, S., Chester, S. A., "Experiments and modeling of the coupled viscoelasticity and Mullins effect in filled rubber materials", Journal of the Mechanics and Physics of Solids, Vol. 188 (2024), 105650.
https://doi.org/10.1016/j.jmps.2024.105650

Alves, A. F. C., Ferreira, B. P., Pires, F. M. A., "A constitutive model for amorphous thermoplastics from low to high strain rates: Formulation and computational aspects", International Journal of Plasticity, Vol. 169 (2023), 103712.
https://doi.org/10.1016/j.ijplas.2023.103712

Anssari-Benam, A., "Hyperinelasticity: An energy-based constitutive modelling approach to isothermal large inelastic deformation of polymers. Part I", Journal of the Mechanics and Physics of Solids, Vol. 192 (2024a), 105790.
https://doi.org/10.1016/j.jmps.2024.105790

Anssari-Benam, A., "Hyperinelasticity. Part II: A stretch-based formulation", Journal of the Mechanics and Physics of Solids, Vol. 192 (2024b), 105825.
https://doi.org/10.1016/j.jmps.2024.105825

Anssari-Benam, A., Hossain, M., "A pseudo-hyperelastic model incorporating the rate effects for isotropic rubber-like materials", Journal of the Mechanics and Physics of Solids, Vol. 179 (2023), 105347.
https://doi.org/10.1016/j.jmps.2023.105347

Anssari-Benam, A., Zaïri, F., "Modelling the finite deformation of thermoplastic polymers via hyperinelasticity. Part I: A semi-crystalline polymer under varying crystallinity ratios and deformation rates", International Journal of Non-Linear Mechanics, International Journal of Non-Linear Mechanics, in press.
https://doi.org/10.1016/j.ijnonlinmec.2025.105091

Apsite, I. Salehi, S., Ionov, L., “Materials for smart soft actuator systems”, Chemical Reviews, Vol. 122 (2022), pp. 1349−1415, DOI: https://doi.org/10.1021/acs.chemrev.1c00453

Argon, A. S., “A Theory for Low-temperature Plastic Deformation of Glassy Polymers”, Philosophical Magazine, Vol. 28 (1973), pp. 839-865.
https://doi.org/10.1080/14786437308220987

Arruda, E. M., Boyce, M. C., “A three-dimensional constitutive model for the large stretch behavior of rubber elastic materials”, Journal of the Mechanics and Physics of Solids, Vol. 41 (1993), pp. 389-412.
https://doi.org/10.1016/0022-5096(93)90013-6

Bosnjak, N., S. Nadimpalli, D. Okumura, S. A. Chester, “Experiments and modeling of the viscoelastic behavior of polymeric gels”, Journal of the Mechanics and Physics of Solids, Vol. 137 (2019), 103829
https://doi.org/10.1016/j.jmps.2019.103829

Boyce, M. C., Parks, D. M., Argon, A. S., “Large inelastic deformation of glassy polymers. Part I: Rate dependent constitutive model”, Mechanics of Materials, Vol. 7 (1988), pp. 15-33.
https://doi.org/10.1016/0167-6636(88)90003-8

Boyce, M. C., Arruda, E. M., “Swelling and mechanical stretching of elastomeric materials”, Mathematics and Mechanics of Solids, Vol. 6 (2001), pp. 641-659.
https://doi.org/10.1177/108128650100600605

Brighenti, R. Montanari, M., Monchetti, S., Hanuhov, T., Spagnoli, A., Cohen, N. “Dependence of stiffness on water content in hydrogels: A statistical mechanics-based framework”, International Journal of Solids and Structures, Vol. 300 (2024) 112920.
https://doi.org/10.1016/j.ijsolstr.2024.112920

Cai, W., Xiao, Z., Sun, T., Wang, J., “A unified viscoelastic constitutive model for studying the mechanical behaviors of polyelectrolyte complex hydrogels with different crosslinker degrees”, Mechanics of Materials, Vol. 189 (2024), 104896.
https://doi.org/10.1016/j.mechmat.2023.104896

Chen, M., Song, G., Ren, B., Cai, L., Hossain, M., Chang, C., “Chiral design of tough spring-shaped hydrogels for smart umbrellas”, Chemical Engineering Journal, Vol. 475 (2023), 146047.
https://doi.org/10.1016/j.cej.2023.146047

Chester, S. A., Anand, L., “A coupled theory of fluid permeation and large deformations for elastomeric materials”, Journal of the Mechanics and Physics of Solids, Vol. 58 (2010), pp. 1879-1906.
https://doi.org/10.1016/j.jmps.2010.07.020

Es-haghi, S. S., Weiss, R. A., “A theory of finite tensile deformation of double-network hydrogels”, Journal of Polymer Science, Vol. 60 (2022), pp. 2476-2487

https://doi.org/10.1002/pol.20220140

Esmaeili, A., George, D., Masters, I., Hossain, M., “Biaxial experimental characterizations of soft polymers: A review”, Polymer Testing, Vol. 128 (2023), 108246.
https://doi.org/10.1016/j.polymertesting.2023.108246

Fazekas, B., Goda, T. J., “Constitutive modelling of rubbers: Mullins effect, residual strain, time-temperature dependence”, International Journal of Mechanical Sciences, Vol. 210 (2021), 106735.
https://doi.org/10.1016/j.ijmecsci.2021.106735

Flory, P. J., Rehner, J., “Statistical mechanics of cross-linked polymer networks II. Swelling”, Journal of Chemistry and Physics, Vol. 11 (1943), pp. 521-526.
https://doi.org/10.1063/1.1723792

Hatami-Marbini, H., Mehr, J. A., “Modeling and experimental investigation of electromechanical properties of scleral tissue; a CEM model using an anisotropic hyperelastic constitutive relation”, Biomechanics and Modeling in Mechanobiology, Vol. 21 (2022), pp. 1325–1337.
https://doi.org/10.1007/s10237-022-01590-5

Haward, R.N., Thackray, G., “The use of a mathematical model to describe isothemal stress-strain curves in glassy thermoplastics”, Proceedings of the Royal Society A, Vol. 302 (1968), pp. 453-472.
https://doi.org/10.1098/rspa.1968.0029

Holzapfel, G. A., “Nonlinear Solid Mechanics: A Continuum Approach for Engineering”, John Wiley and Sons Ltd, Chichester, England (2000), pp. 161-176.

Javadi, M. H., Darijani, H., Niknafs, M., “Constitutive modeling of visco-hyperelastic behavior of double-network hydrogels using long-term memory theory”, Journal of Applied Polymer Science, Vol. 138 (2021), 49894.
https://doi.org/10.1002/app.49894

Jin, X., Wei, C., Wu, C., Zhang, W., “Gastric fluid-induced double network hydrogel with high swelling ratio and long-term mechanical stability”, Composites Part B, Vol. 236 (2022), 109816.
https://doi.org/10.1016/j.compositesb.2022.109816

Kawai, R., Tanaka, H., Matsubara, S., Ida, S., Uchida, M., Okumura, D., “Implicit rule on the elastic function of a swollen polyacrylamide hydrogel”, Soft Matter, Vol. 17 (2021), pp. 4979–4988.
https://doi.org/10.1039/D1SM00346A

Khalid, M. Y., Arif, Z. U., Tariq, A., Hossain, M., Khan, K. A., Umer, R., “3D printing of magneto-active smart materials for advanced actuators and soft robotics applications”, European Polymer Journal, Vol. 205 (2024), 112718,
https://doi.org/10.1016/j.eurpolymj.2023.112718

Khiêm, V. N., Mai, T. T., Urayama, K., Gong, J. P., Itskov, M., “A multiaxial theory of double network hydrogels”, Macromolecules, Vol. 52 (2019), pp. 5937−5947.

https://doi.org/10.1021/acs.macromol.9b01044

Kikuchi, S., Matsubara, S., Nagashima, S., Okumura, D., “Diversity of the bifurcations and deformations on films bonded to soft substrates: Robustness of the herringbone pattern and its cognate patterns”, Journal of the Mechanics and Physics of Solids, Vol. 159 (2022), 104757.
https://doi.org/10.1016/j.jmps.2021.104757

Kuhn, W., Grün, F., “Beziehungen zwischen elastischen Konstanten und Dehnungsdoppelbrechung hochelastischer Stoffe”, Kolloid-Zeitschrift und Zeitschrift für Polymere, Vol. 101 (1942), pp. 248-271 (in German).
https://doi.org/10.1007/BF01793684

Lan, T., Jiang, Y., Wu, P., “A thermodynamically-based constitutive theory for amorphous glassy polymers at finite deformations”, International Journal of Plasticity, Vol. 158 (2022), 103415.
https://doi.org/10.1016/j.ijplas.2022.103415

Lan, T., Shao, T., Zhang, Y., Zhang, Y., Zhu, J., Jiang Y., Wu, P., “A physically-based constitutive model for amorphous glassy polymers in large deformations”, European Journal of Mechanics / A Solids, Vol. 104 (2024), 105015.
https://doi.org/10.1016/j.euromechsol.2023.105015

Lei, J, Zhou, Z., Liu, Z., “Side Chains and the Insufficient lubrication of water in Polyacrylamide Hydrogel—A New Insight”, Polymers, Vol. 22 (2019), 1845
https://doi:10.3390/polym11111845

Lei, J., Li, Z., Xu, S., Liu, Z., “Recent advances of hydrogel network models for studies on mechanical behaviors”, Acta Mechanica Sinica, Vol. 37 (2021), pp. 367–386.
https://doi.org/10.1007/s10409-021-01058-2

Li, Z., Kadapa, C., Hossain, M., Wang, J., “A numerical framework for the simulation of coupled electromechanical growth”, Computer Methods in Applied Mechanics and Engineering, Vol. 414 (2023), 116128.
https://doi.org/10.1016/j.cma.2023.116128

Lin, R., Xu, S., Liu, Z., “A visco-hyperelastic model for hydrogels with different water content and its finite element implementation”, International Journal of Solids and Structures, Vol. 293 (2024), 112761.
https://doi.org/10.1016/j.ijsolstr.2024.112761

Mao, Y., Lin, S., Zhao, X., Anand, L., “A large deformation viscoelastic model for double-network hydrogels”, Journal of the Mechanics and Physics of Solids, Vol. 100 (2017), pp. 103–130.
http://dx.doi.org/10.1016/j.jmps.2016.12.011

Matsubara, S., Takashima, A., Nagashima, S., Ida, S., Tanaka, H., Uchida, M., Okumura, D. “Time-swelling superposition principle for the linear viscoelastic properties of polyacrylamide hydrogels”, Advanced Structured Materials, Vol. 194 (2023), pp. 175–204.

https://doi.org/10.1007/978-3-031-39070-8_12

Nagashima, S., Akamatsu, N., Cheng, X., Matsubara, S., Ida, S., Tanaka, H., Uchida, M., Okumura, D., “Self-wrinkling in polyacrylamide hydrogel bilayers”, Langmuir, Vol. 39 (2023), pp. 3942−3950.
https://doi.org/10.1021/acs.langmuir.2c03264

Ogden, R. W., “Large deformation isotropic elasticity – on the correlation of theory and experiment for incompressible rubberlike solids”, Proceedings of the Royal Society A, Vol. 326 (1972), pp. 565-584.
https://doi.org/10.1098/rspa.1972.0026

Okumura, D., Kondo, A. Ohno, N., “Using two scaling exponents to describe the mechanical properties of swollen elastomers”, Journal of Mechanics and Physics of Solids, Vol. 90 (2016), pp. 61–76.
https://doi.org/10.1016/j.jmps.2016.02.017

Okumura, D., Mizutani, M., Tanaka, H., Uchida, M., “Effects of two scaling exponents on biaxial deformation and mass transport of swollen elastomers”, International Journal of Mechanical Sciences, Vol. 3 (2018), pp. 135-140.
https://doi.org/10.1016/j.ijmecsci.2017.08.042

Okumura, D. Chester, S. A., “Ultimate swelling described by limiting chain extensibility of swollen elastomers”, International Journal of Mechanical Sciences, Vol 144, (2018), pp. 531-539.
https://doi.org/10.1016/j.ijmecsci.2018.06.011

Sridhar, S. L., Vernerey, F. J., “Mechanics of transiently cross-linked nematic networks”, Journal of the Mechanics and Physics of Solids, Vol. 141 (2020), 104021.
https://doi.org/10.1016/j.jmps.2020.104021

Tayeb, A., Arfaoui, M., Zine, A., Ichchou, M., Hamdi, A., Abdallah, J. B., “Investigation of the nonlinear hyper-viscoelastic behavior of elastomers at finite strain: implementation and numerical validation”, The European Physical Journal Plus, Vol. 137 (23022), 536.
https://doi.org/10.1140/epjp/s13360-022-02757-w

Tanaka, F., Edwards, S. F., “Viscoelastic properties of physically crosslinked networks. 1. Transient network theory”, Macromolecules, Vol. 25 (1992), pp. 1516–1523.
https://doi.org/10.1021/ma00031a024

Uchida, M., Tada N., “Sequential evaluation of continuous deformation field of semi-crystalline polymers during tensile deformation accompanied by neck propagation”, International Journal of Plasticity, Vol. 27 (2011), pp. 2085–2102.
https://doi.org/10.1016/j.ijplas.2011.07.009

Uchida, M., Sengoku, T., Kaneko, Y., Okumura, D., Tanaka, H., Ida, S., “Evaluation of the effects of cross-linking and swelling on the mechanical behaviors of hydrogels using the digital image correlation method”, Soft Matter, Vol. 15 (2019a), pp. 3389-3396.

https://doi.org/10.1039/C9SM00049F.

Uchida, M., Wakuda, R., Kaneko, Y., “Evaluation and modeling of mechanical behaviors of thermosetting polymer under monotonic and cyclic tensile tests”, Polymer, Vol. 174 (2019b), pp. 130–142.
https://doi.org/10.1016/j.polymer.2019.04.064

Uchida, M., Kamimura, K., Yoshida, T., Kaneko, Y., “Viscoelastic-viscoplastic modeling of epoxy based on transient network theory”, International Journal of Plasticity, Vol. 153 (2022), 103262.
https://doi.org/10.1016/j.ijplas.2022.103262

Uchida, M., Yoshida, T., Okada, E., Touji, M., Kaneko, Y., “Mechanical modeling of polyamide 6 obtained from different thermal histories”, Polymer, Vol. 296 (2024), 126770.
https://doi.org/10.1016/j.polymer.2024.126770.

Vernerey, F. J., Long, R., Brighenti, R., “A statistically-based continuum theory for polymers with transient networks”, Journal of the Mechanics and Physics of Solids, Vol. 107 (2017), pp. 1-20.
https://doi.org/10.1016/j.jmps.2017.05.016

Xiao, R., Mai, T. T., Urayama, K., Gong, J. P., Qu, S., “Micromechanical modeling of the multi-axial deformation behavior in double network hydrogels”, International Journal of Plasticity, Vol. 137 (2021), 102901.
https://doi.org/10.1016/j.ijplas.2020.102901

Yoshida, T., Nakane, T., Uchida, M., Kaneko, Y., “Mechanical modeling and testing of different polyamides considering molecular chain structure, crystallinity, and large strains”, International Journal of Solids and Structures, Vols. 239–240 (2022), 111419.
https://doi.org/10.1016/j.ijsolstr.2021.111419

Zhan, L., Qu. S, Xiao, R., “A Review on the Mullins Effect in Tough Elastomers and Gels”, Acta Mechanica Solida Sinica, Vol. 37 (2024), pp. 181–214
https://doi.org/10.1007/s10338-023-00460-6

Zhu, P., Zhong, Z., “Modelling the mechanical behaviors of double-network hydrogels”, International Journal of Solids and Structures, Vols. 193–194 (2020), pp. 492–501.
https://doi.org/10.1016/j.ijsolstr.2020.03.003